## Materials and Methods

### Nanofabrication and characterization of glass substrates

Glass coverslips (25 mm diameter, 0.17 mm thickness, No. 1.5; Harvard Apparatus) were cleaned by sonication in isopropanol/water (1:1 volume) for 30 min, rinsed with a stream of ultrapure water, cleaned with piranha solution (conc. $H_2SO_4$/H2O2 (30%), 3:1 volume) for 5 min at room temperature, rinsed with a stream of ultrapure water, and dried with a flow of nitrogen. A thin film of chromium (6 nm) as a conductive layer was deposited on the cleaned coverslip by an e-beam metal evaporator (Edwards EB3) with 0.1-0.5 nm/sec deposition rate. Nanocurvature was fabricated on the coverslip with a focused ion beam (FIB; FEI Quanta) operated at 30 kV and 1 nA using a cylindrical milling shape of 100 nm in diameter and 100 nm in depth. The chromium film was removed by immersing the coverslip in concentrated HCl aq. and touching the surface with an aluminum wire. The coverslip was rinsed with deionized water and dried with a flow of nitrogen. The resulting geometry was measured by atomic force microscopy (AFM; Asylum Research MFP-3D) at a tapping mode with 335 kHz frequency.

### invSLB formation

A lipid stock solution in chloroform (Avanti polar lipids, Alabama, US) was mixed to yield the composition of interest. POPC (1-palmitoyl-2-oleoyl-sn-glycero-3-phosphocholine) and POPS (1-palmitoyl-2-oleoyl-sn-glycero-3-phospho-L-serine) were from Avanti polar lipids (Alabama, USA). PI(3)P (Dipalmitoyl phosphatidylinositol 3-phosphate) was from Echelon bioscience (Utah, USA). DiD was from Life Technologies (CA, USA). The composition used in all experiments was POPC:POPS:PI(3)P:DiD = 82:15:3:0.005 except where specified otherwise. For quantitation of PS distribution, the labeled lipid TopFluor-PS (1-palmitoyl-2-(dipyrrometheneboron difluoride)undecanoyl-sn-glycero-3-phospho-L-serine; Avanti Polar Lipids, Alabama, US) was used. The lipid mixtures were dried on a piranha etched round bottom flask under nitrogen, followed by overnight incubation in a vacuum chamber. Milli-Q filtered water (EMD Millipore, MA, USA) was added to reach 2 mg/ml total lipid concentration. Freezing and thawing was repeated three times to hydrate lipids into water. A hand held extruder (Avanti polar lipids, Alabama, US) was used to extrude lipids through a 100 nm sized filter (Whatman, PA, USA) nine times. The extruder was cleaned by 30 min sonication in 1%

Hellmanex (Hellma analytics) followed by another 30 min in water before use. Liposomes were kept at 4 ˚C and were used within one day.

Nanofabricated glass substrates were cleaned with piranha solution (concentrated sulfuric acid: hydrogen peroxide = 3:1) before each use. Clean substrates were assembled into the Attofluor cell chambers (Life technologies, CA, USA). Liposome solutions were mixed with 1x PBS solution containing 5 mM $MgCl_2$ at a 1:1 ratio, and the solution was incubated on top of glass substrates for one hour. The samples were washed by exchanging buffer five times without exposing the lipid membrane surface to air, and the SLB was used immediately after preparation. The solution phase buffer 150mM NaCl, 50mM Tris, pH 7.4 was used throughout unless specified otherwise. Membrane fluidity was checked before starting each experiment. Nanofabricated glass substrates were reused up to three times by thoroughly washing with 1% detergent solution and isopropyl alcohol. Repeated reuse of substrate more than five times resulted in the formation of immobile bilayers, and therefore the substrates were discarded after three uses. We found our supported lipid bilayer system becomes immobile after ~1 hour from its formation as detected by FRAP experiments, suggesting instability of the highly charged supported lipid bilayer system over longer time scales. The bilayer was stable without change of membrane properties within the time window of all experiments carried out in this report.

For the $His_6$-tethered control experiments shown in Figure 2, 1% Ni-DOGS lipids replaced an equivalent amount of POPC. After the initial formation of the SLB, the bilayer was incubated with 100 mM NiCl for 5 min, washed, then incubated with 10nM $His_6$-tagged proteins for 30 min. Ni-DOGS (1,2-dioleoyl-sn-glycero-3-[(N-(5-amino-1-carboxypentyl) iminodiacetic acid)succinyl]) was from Avanti Polar Lipids.

**Protein expression and purification**

Protein expression and purification was carried out as previously described (1). Briefly, the human ESCRT-II complex was expressed in *E. coli* as a TEV protease-cleavable $His_6$ fusion protein (2) and labeled on native lysine residues using Atto488 NHS ester (Sigma-Aldrich, MO, USA). Human and yeast ESCRT-III subunits were expressed and purified as previously described (1), and labeled with Atto488 maleimide (Sigma-Aldrich) on engineered unique cysteine residues. The SNX1 BAR domain and 88-522 construct were purified as previously described (3). Briefly, they were expressed as MBP fusion proteins in *E. Coli* and the tags were

removed by TEV protease cleavage of the linker region. Tag fragments were removed by Ni-NTA beads followed by Superdex 200 (GE Healthcare) purification. Purified proteins were fluorescently labeled by incubating with a 10-fold molar excess of Alexa488 NHS ester for non-specific labeling at 4 ˚C overnight. Excess dye was removed with a HiTrap desalting column (GE Healthcare). The labeling ratio was in the range of 0.5-1.0 dye per protein.

**TIRF imaging**

TIRF microscopy was performed with a Nikon Ti-E based microscope (Nikon, Tokyo, Japan) with an ASI automatic stage (Applied Scientific Instrumentation, OR, USA). The excitation laser source was an OPSL smart laser module (Coherent, CA, USA) coupled to the microscope by optical fibers of an ILE merge module (Spectra Physics, CA, USA) with fixed fiber alignment. Excitation wavelengths of 488, 532, 640 nm were used. Laser intensity was voltage controlled from the controlling computer. Chroma optical filter sets (Chroma technology, VT, USA) of excitation dichroic, excitation wavelength filter, emission wavelength filters for each TIRF wavelength were used. A 100X TIRF NA1.49 oil objective (Nikon) was used with 1.5x emission path magnification. An Andor Ixon Ultra EMCCD camera with 512 x 512 pixels (Andor Technology, Belfast, UK) was used for image acquisition without electron multiplication gain. An emission filter wheel (Sutter Instrument, CA, USA) with emission bandwidth filters was used for noise elimination. The whole setup was installed on a gas floated vibration isolation table (TMC, CA, USA). All devices were automatically controlled from the controlling computer by Micro manager, an ImageJ based software (https://www.micro-manager.org/).

Laser power used was ~12mW (488 nm), ~3mW (532 nm), ~6mW (640 nm) for each wavelength excitation as measured right before the objective. The TIRF angle was adjusted to ensure surface-specific excitation. The image acquisition time was 100 ms for all data shown unless specified otherwise. Multi-color imaging was always performed from higher to lower wavelength excitation. Sample chambers were firmly held by the stage adaptor to minimize mechanical drift during time lapse imaging. A perfect focus system (Nikon) prevented loss of focus during the time lapse imaging. An oxygen scavenger system (4) consisting of glucose, glucose oxidase and catalase (all from Sigma-Aldrich) was added right before imaging to minimize photobleaching.

The slightly higher DiD intensity observed by TIRF near the invaginations can be

accounted for by the higher area density of fluorophores as projected onto a plane. Given a half ellipsoidal shape with radius of r=200nm and depth d=100nm, the surface area of an invagination is 1.38 of the corresponding flat region, from $2\pi r \left(\frac{(r*r)^{1.6}+2(r*d)^{1.6}}{3}\right)^{1/1.6} / \pi r^2 = 1.38$. We observe that the DiD emission intensity in invaginations is ~1.5-fold greater than the surrounding flat membrane (Fig. 1D) consistent with this topography.

**SIM imaging**

Structured illumination microscopy (SIM) was performed using an ELYRA SR.1 Superresolution Microscopy (Zeiss, Oberkochen, Germany) instrument. A 100x oil objective was used with 1.6x final magnification. A sCMOS camera was used to collect the signal for the SIM mode. 488nm laser excitation SIM mode data acquisition was performed for each time point after initiating the reaction. The Z-position was manually focused for each acquisition to use as a z-stack center. Images were acquired as z-stacks of a 0.1 µm step spanning 1 µm, with the focal point as the z-scan center. Images were acquired from 3 different grating illumination patterns that are 120 µm from each other with a 200 ms exposure time to complete one set of full SIM acquisition. Sets of images were later constructed into complete images by the automated SIM analysis of the software ZEN white (Zeiss).

**Data analysis**

ImageJ (http://imagej.nih.gov/ij/) was used for image analysis. For quantification of total intensity in each invagination, n > 60 invaginations in at least six different images from different positions were analyzed. A fixed size circular region of interest was used for the same set of data. For kinetic analysis, same strategy was used for the each image across the entire time window. For time lapse studies, n=30 invaginations from six image stacks from different positions were analyzed. Radial analysis of Figure 7C was performed as an automated image analysis in Matlab R2014b (Mathworks, MA, USA). Center positions for invaginations (n=67) were manually determined by examining images to generate lists of Cartesian coordinates. Intensity values and distances of pixels around the centers were collected and binned by distance. Total intensity summation was divided by the number of pixels in the bin to obtain the final

average intensity value for each distance bin. Each data point of Figure 7C was plotted at the mean distance of each distance bin in x axis.

**Deterministic nucleation growth model**

The set of ordinary differential equations (ODE) was solved numerically using the ode45 function in Matlab R2014b (Mathworks, MA, USA). ODEs describing the elementary chemical reactions were adapted from a model previously applied to the nucleation and growth of amyloid fibers (5). The nucleation step generates the polymer elongation ends, E. Multimer-dependent nucleation is of order *m* with respect to the non-monomer concentration.

$$\frac{d[E]}{dt} = k_n[A_1]^n([A_{tot}] - [A_1])^m$$

Here, [E] denotes concentration of elongation ends, $[A_1]$ is monomer concentration, $[A_{tot}]$ is total protein concentration, and $k_n$ is the rate constant of nucleation reaction. We used $n = 1$, however, varying $n$ from 0 to 2 did not alter the general trends of the sigmoidal growth with variations in absolute values. We found that $m = 1$, which is the same order as the original model we adapted from, provided good fits to the data. Polymer elongation takes the form of reaction between elongation ends and monomers:

$$\frac{d[A_1]}{dt} = -k_e[E][A_1]$$

Here, $k_e$ is the kinetic constant of elongation. The concentration of polymer on the membrane, [Multimer] = $[A_{tot}]$-$[A_1]$, is equivalent to the fluorescence intensity in our experiments. The initial condition was set accordingly for each constant $K = ([A_{tot}] - [A_1])/[A_1]$, $[A_1]_0 = [A_{tot}]/(1 + K)$ , and $[E]_0 = 0$. $[A_{tot}]$ was determined from experimental values. Nonlinear parameter optimization was performed by nlinfit function in Matlab as a simultaneous three parameter ($K$, $k_n$, $k_e$) optimization problem with respect to the experimental data. $([A_{tot}] - [A_1])$ was treated as the fluorescence readout of multimer formation. The background signal was subtracted beforehand.

**Supplementary Figure legends**

**Figure S1. Characterization of invaginated supported lipid bilayers (invSLBs).**
(A) Sample line profiles of the nano-fabricated glass surface. The geometries shown are actual morphologies measured by atomic force microscopy. Each panel a, b, c was obtained from a scan along one of lines shown in (B). (B) AFM measurements on FIB fabricated substrates. The upper orange colored lines indicate the scans shown in (A) and the yellow colored box indicates the region shown in the surface plot in Figure 1C.

**Figure S2. PS is uniformly distributed on invSLBs.**
Sample TIRF image and line profile of POPC:POPS:PI(3)P:DiD:TopFluor-PS 82:15:3:0.005:0.005 on invSLB.

**Figure S3. Control experiments for invagination specific recruitment and line intensity profiles of ubiquitin, BAR and SNX1 88-522.**
(A) TIRF image after 20 min incubation of 400 nM ubiquitin-Atto488 (no $His_6$ tag) as a control for non-specific recruitment. Atto488 fluorescence contrast was scaled exactly the same as in Figure 2A for direct comparison. (B) TIRF image after 20 min incubation of 100 nM BSA-Cy3. Blue indicates membrane-tethered $His_6$-ubiquitin-Cy5 as a control for membrane binding induced recruitment. Scale bars are 5 μm. (C) TIRF fluorescence image after 20 min incubation of 400 nM BAR-Alexa488. (D) TIRF fluorescence image after 20 min incubation of 400 nM SNX1 88-522-Alexa488. (C) and (D) were scaled the same as (A) for direct comparison. Representative intensity profiles (yellow lines) from the 400 nM incubation of (E) Ubiquitin-Atto488, (F) BAR-Alexa488 and (G) SNX1 88-522-Alexa488 with PC, PS, and PI3P. Intensity values are shown as raw values. Scale bars are 5μm.

**Figure S4. Time lapse images for the sigmoidal kinetics of CHMP4B recruitment to invaginations.**
Representative time lapse images for the (A) 40nM, and (B) 4nM CHMP4B-Atto488 experiments of the Figure 3. Scale bars are 5 μm.

**Figure S5. Time lapse images for ESCRT-II and CHMP6 promoted CHMP4B nucleation.**
Representative time lapse images of the (A) CHMP6+ CHMP4B-Atto488 and (B) CHMP4B-Atto488 experiments of the Figure 4. Further images are shown in Figure S4.Scale bars are 5 μm.

**Figure S6. Single invagination analysis of lag time distribution.**
Lag times of individual invagination assemblies were calculated from the data shown in Figure 4B. Lag times were quantified by fitting each individual trace with a general sigmoidal equation $y = y_0 + y_m(1/\exp(\frac{t_{lag}-x}{r}))$ where $y_0$ and $y_m$ denote offset and maximum y values each. $t_{lag}$ is the lag time and r is an arbitrary rate constant. Relatively narrow distribution of lag time compared to the difference between averages at different conditions suggests the event within an invatination is from sufficiently large number of molecules that the average behavior over all invaginations can be well approximated by single invagination kinetics. We attribute the slightly greater variation in the case of ESCRT-II, CHMP6 and CHMP4B to the very short lag time, resulting in the truncation of earliest part of the sigmoidal kinetics in some cases.

**Figure S7. Lag time distribution for nucleation on flat and invaginated membranes.**
Lag times of individual assembly initiation were calculated from the experiment shown in Figure 5C. N=35 initiation events on flat membrane region were examined manually to study intensity traces similar to Figure 5E. Lag times were defined and quantified by manually determining the very first time point of steep intensity increase. Quantified intensity histogram is shown as green bars. Invagination assisted initiation was already complete for all invaginations within a minute of incubation as indicated by a gray bar. Lag times are widely distributed within 30 min time window of observation suggesting stochastic nature of the events on flat lipid bilayers while invagination geometry dramatically catalyzes the initiation of overgrowth.

**Figure S8. SIM images after 30 min incubation without photo-bleaching.**
Representative SIM images after 30 min incubation in the dark.

**References**


1. Carlson LA & Hurley JH (2012) In Vitro Reconstitution of the Ordered Assembly of the ESCRT Machinery at Membrane-Bound HIV-1 Gag Clusters. *Proc Natl Acad Sci U S A* 109:16928-16933.
2. Im YJ & Hurley JH (2008) Integrated structural model and membrane targeting mechanism of the human ESCRT-II complex. *Dev Cell* 14:902-913.
3. van Weering JRT*, et al.* (2012) Molecular basis for SNX-BAR-mediated assembly of distinct endosomal sorting tubules. *EMBO J.* 31(23):4466-4480.
4. Rasnik I, McKinney SA, & Ha T (2006) Nonblinking and long-lasting single-molecule fluorescence imaging. *Nat Meth* 3(11):891-893.
5. Ruschak AM & Miranker AD (2007) Fiber-dependent amyloid formation as catalysis of an existing reaction pathway. *Proceedings of the National Academy of Sciences* 104(30):12341-12346.

A

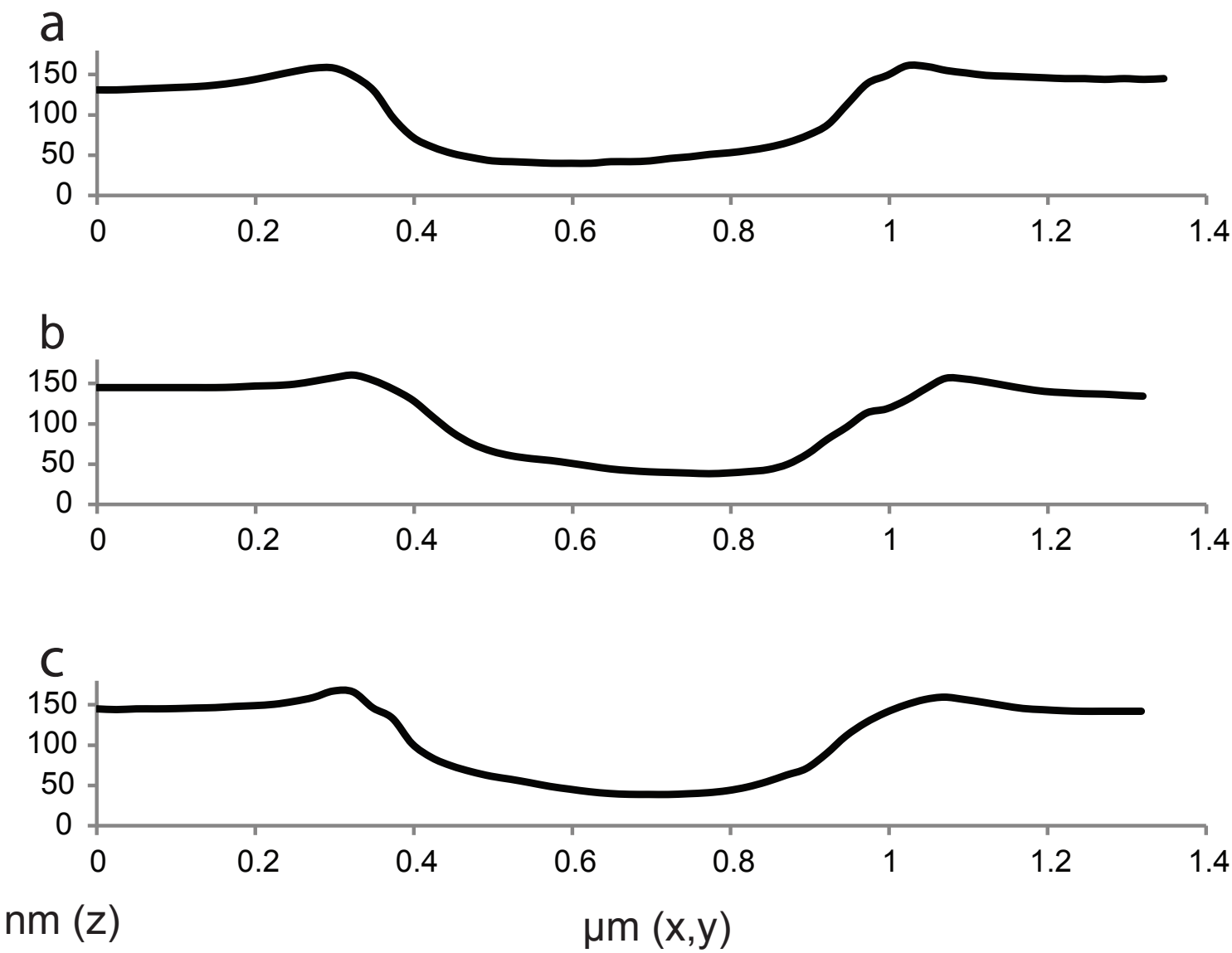
a
150
100
50
0
0
0.2
0.4
0.6
0.8
1
1.2
1.4
b
150
100
50
0
0
0.2
0.4
0.6
0.8
1
1.2
1.4
c
150
100
50
0
0
0.2
0.4
0.6
0.8
1
1.2
1.4
nm (z)
µm (x,y)

B

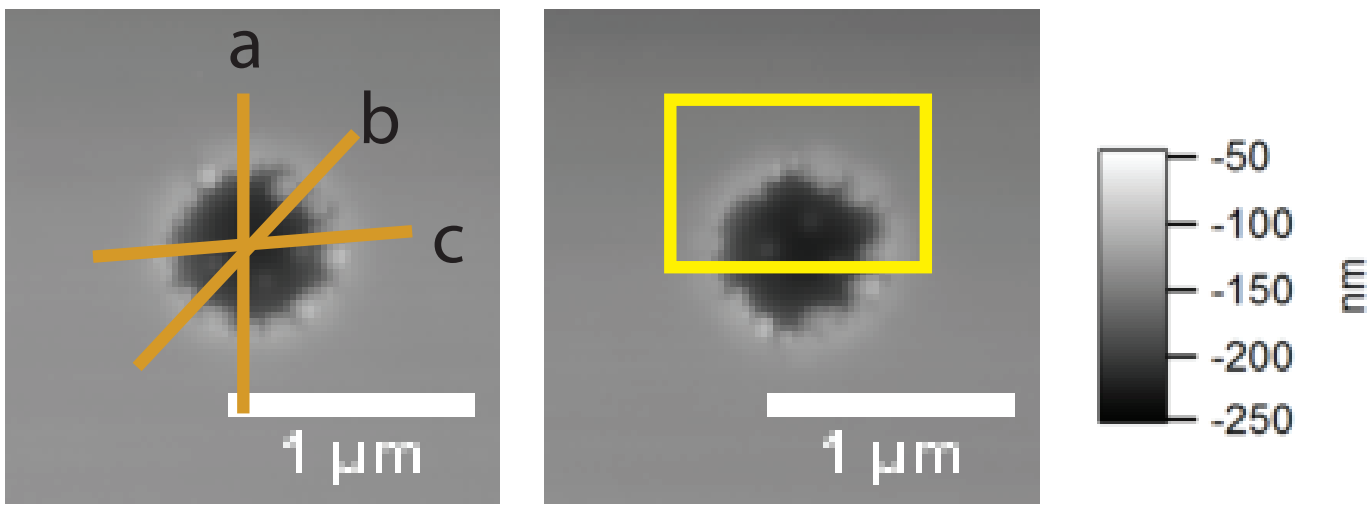
a
b
c
1 µm
1 µm
-50
-100
-150
-200
-250
nm

Figure S1

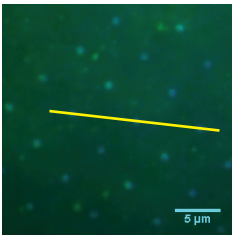
5 µm

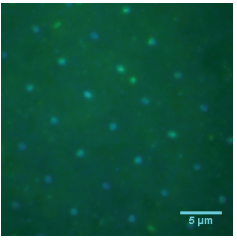
5 µm

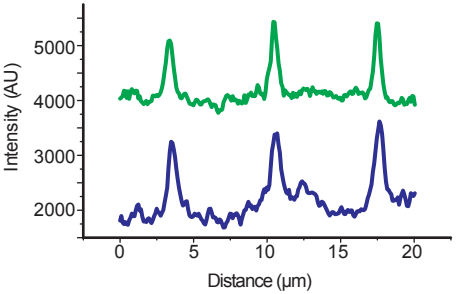
Intensity (AU)
5000
4000
3000
2000
0
5
10
15
20
Distance (µm)
TopFluor-PS
DiD

Figure S2

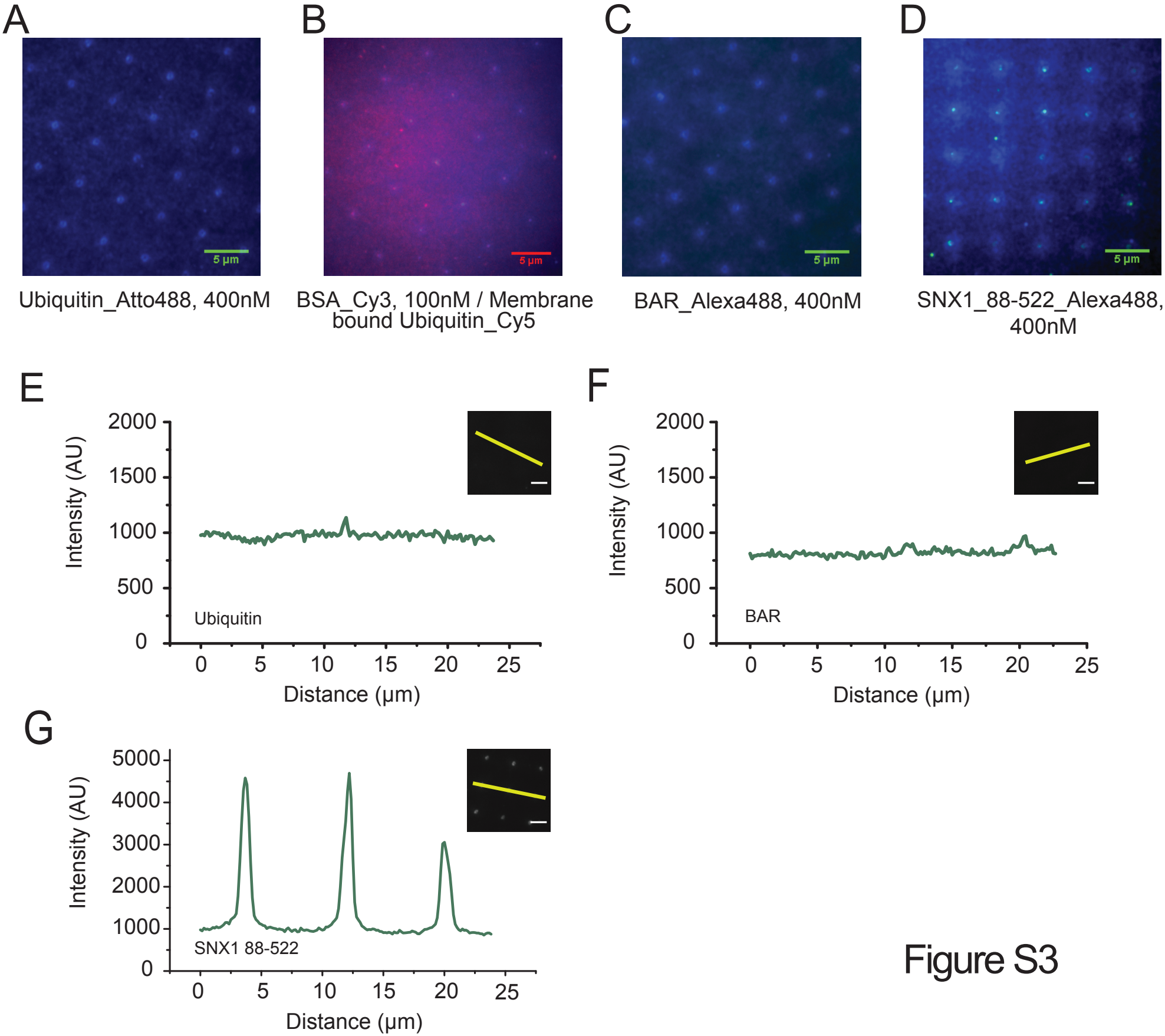
A
B
C
D
5 µm
Ubiquitin_Atto488, 400nM
BSA_Cy3, 100nM / Membrane bound Ubiquitin_Cy5
BAR_Alexa488, 400nM
SNX1_88-522_Alexa488, 400nM
E
F
G
Intensity (AU)
Distance (µm)
Ubiquitin
BAR
SNX1 88-522
0
500
1000
1500
2000
2000
3000
4000
5000
0
5
10
15
20
25

Figure S3

A

40 nM

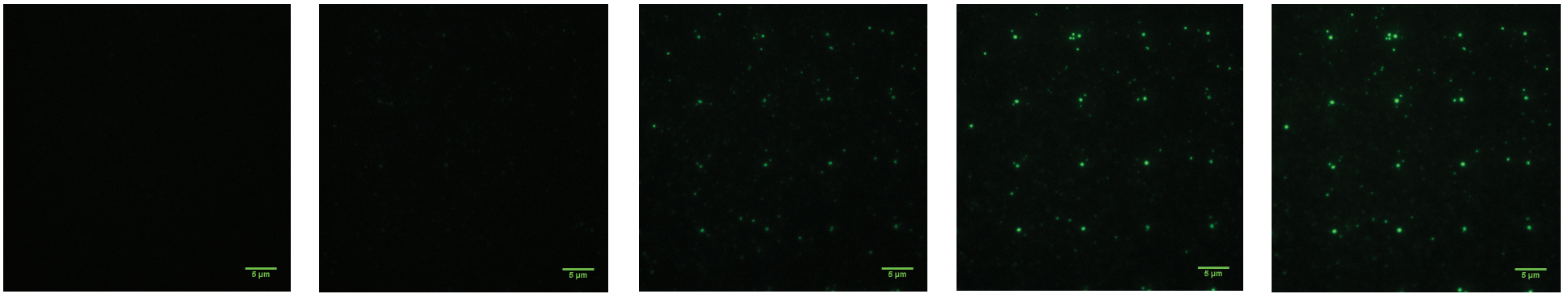

0 min 2 min 4 min 6 min 8 min

B

4 nM

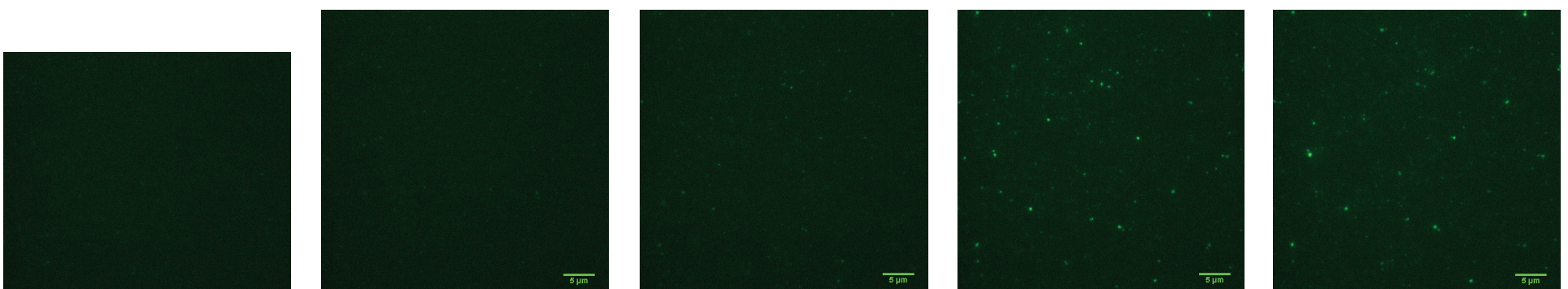

0 min 4 min 8 min 12 min 16 min

Figure S4

A

CHMP6 + CHMP4B

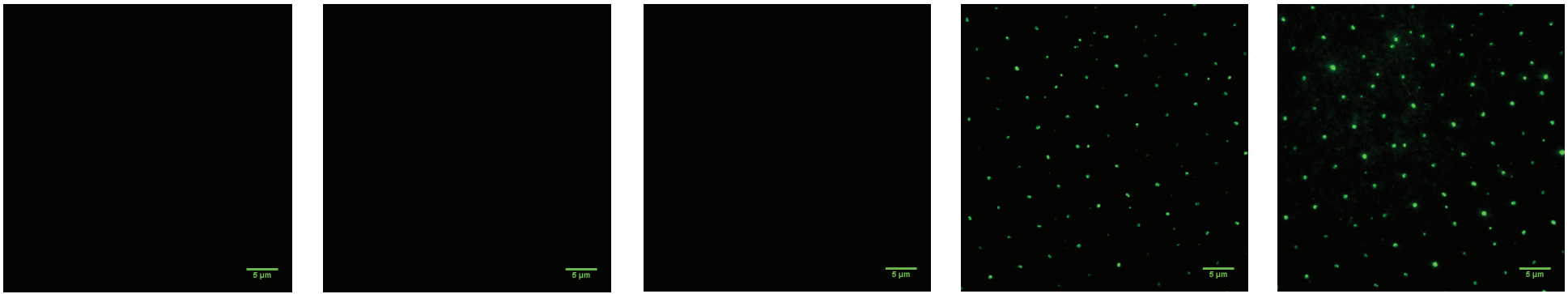


0 min 3 min 6 min 9 min 12 min

B

CHMP4B

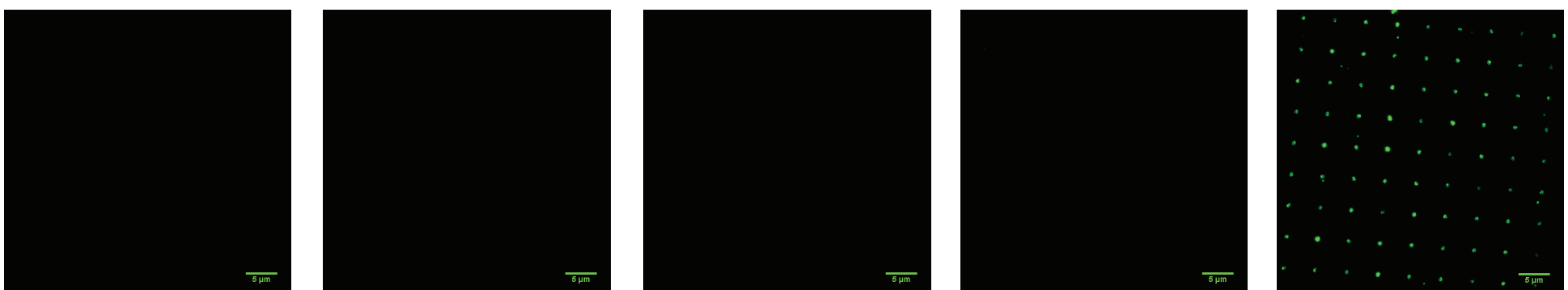


0 min 4 min 8 min 12 min 16 min

Figure S5

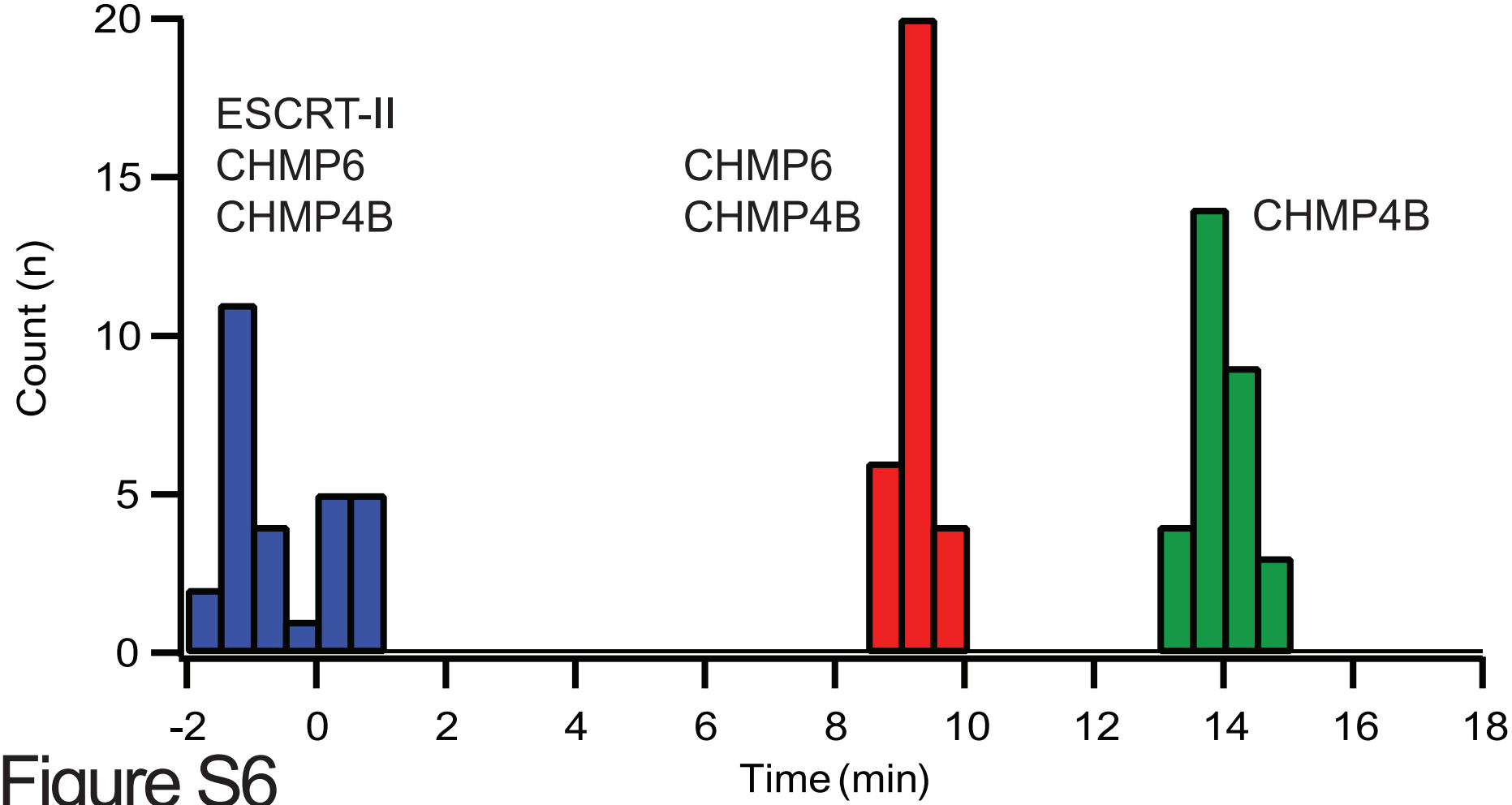
20
15
10
5
0
Count (n)
ESCRT-II
CHMP6
CHMP4B
CHMP6
CHMP4B
CHMP4B
-2
0
2
4
6
8
10
12
14
16
18
Time (min)

Figure S6

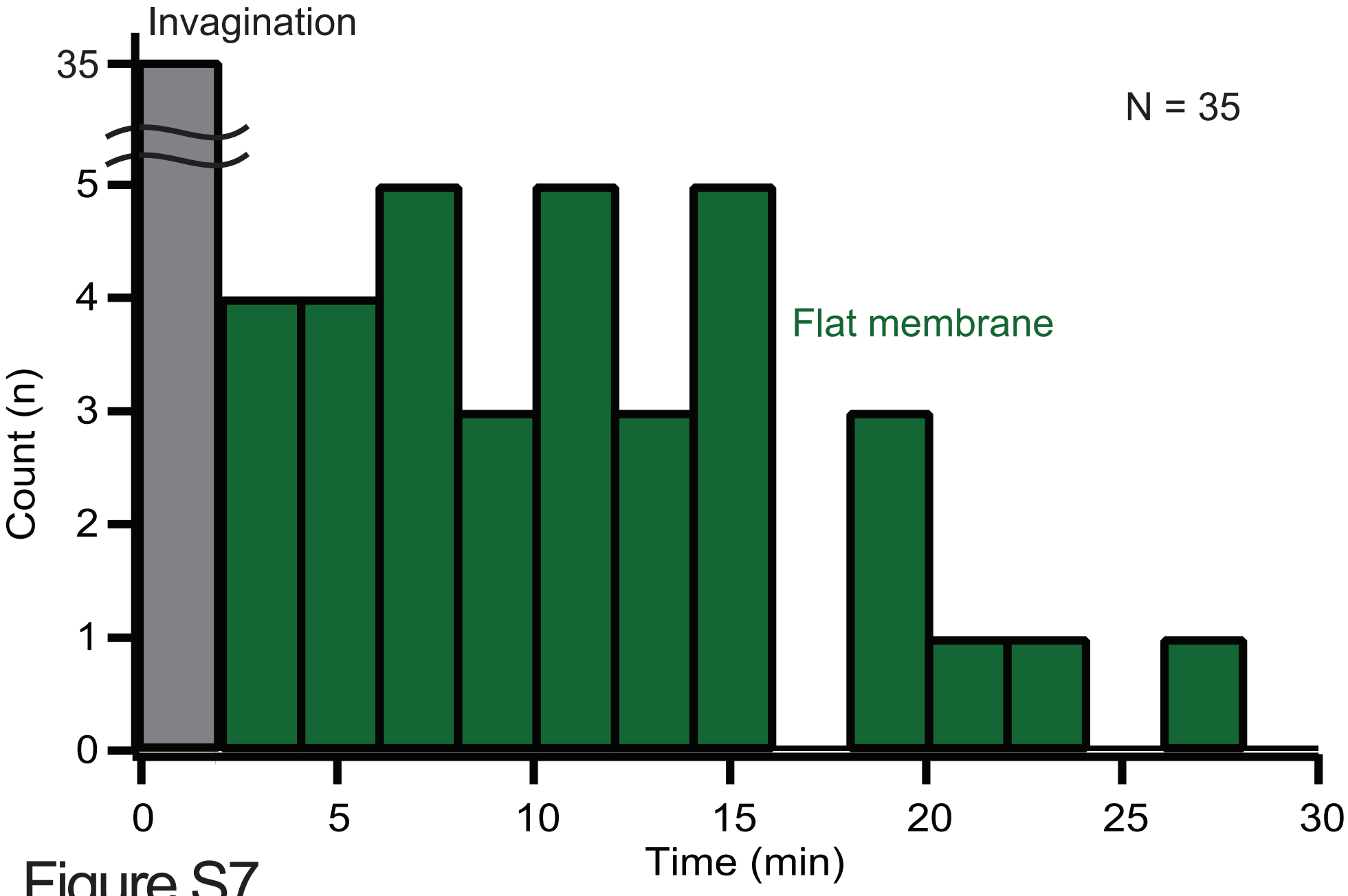
Invagination
35
5
4
3
2
1
0
N = 35
Flat membrane
Count (n)
0
5
10
15
20
25
30
Time (min)

Figure S7

Snf7 SIM

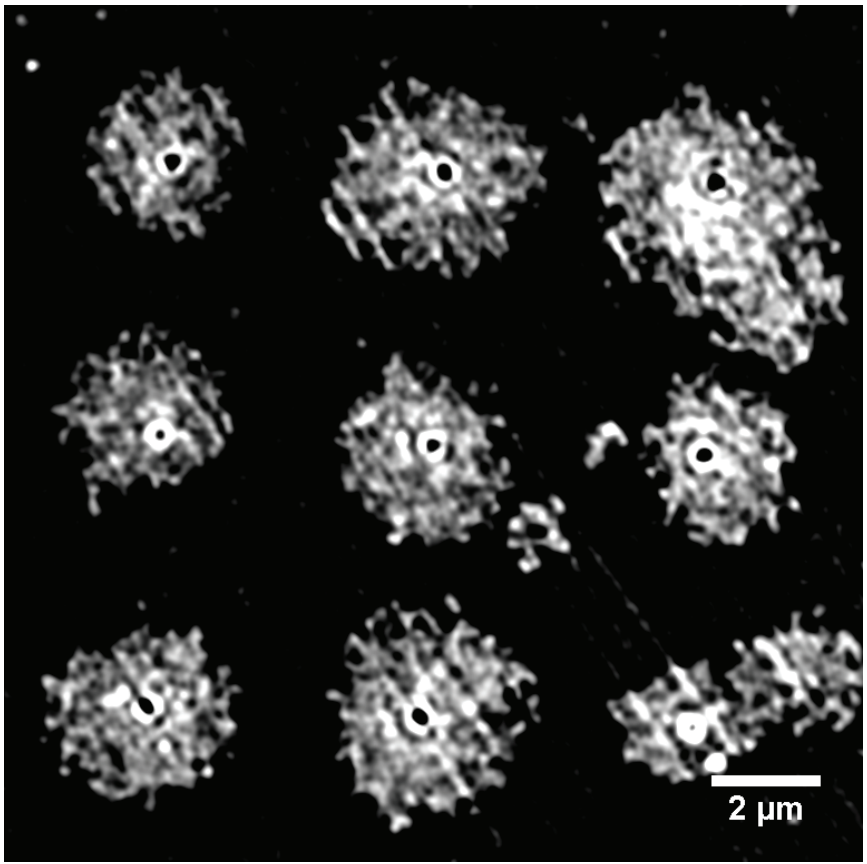


Image 1

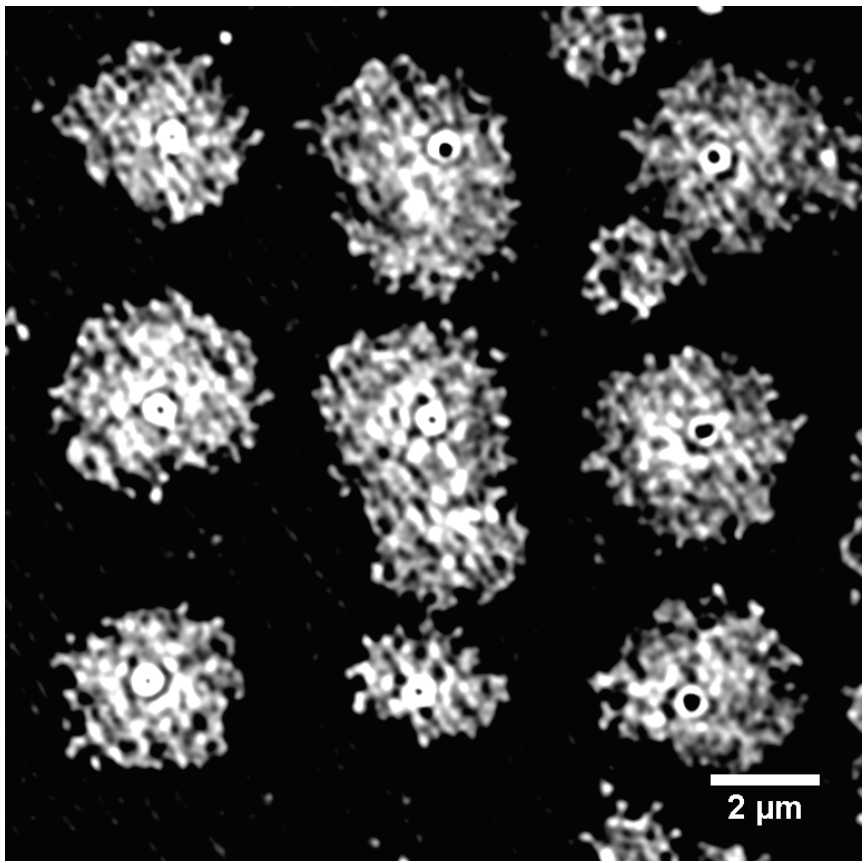


Image 2

Figure S8

**Table S1. Parameters for concentration dependence of CHMP4 assembly**

| | ESCRT-II (nM) | CHMP6 (nM) | CHMP4B (nM) | K ($10^{-3}$) | $k_n$ ($10^{-5}$ $min^{-1}$) | $k_e$ ($10^{-1}$ $min^{-1}$) | $A_{tot}$ (Unitless) |
|---|---|---|---|---|---|---|---|
| **Experiment 1** | 100 | 200 | 4 | 3.83 | 12.6 | 15.4 | 45 |
| **Experiment 2** | 100 | 200 | 40 | 51.3 | 4.01 | 1.79 | 300 |
| **Experiment 3** | 100 | 200 | 400 | 226 | 3.83 | 2.48 | 1300 |

The first three columns indicate the concentration of each protein used in the experiment, and the final four columns show kinetic parameters obtained by optimizing the mathematical model (Equation 1-2) to fit the data from each experiment.

**Table S2. Parameters for CHMP6 and ESCRT-II dependence of CHMP4 assembly**

| | ESCRT-II (nM) | CHMP6 (nM) | CHMP4B (nM) | K ($10^{-3}$) | $k_n$ ($10^{-5}$ $min^{-1}$) | $k_e$ ($10^{-1}$ $min^{-1}$) | $A_{tot}$ (Unitless) |
|---|---|---|---|---|---|---|---|
| **Experiment 1** | 0 | 0 | 40 | 0.0114 | 9.85 | 1.20 | 255 |
| **Experiment 2** | 0 | 200 | 40 | 2.18 | 5.56 | 0.962 | 310 |
| **Experiment 3** | 100 | 200 | 40 | 335 | 8.12 | 3.18 | 500 |

Concentrations and kinetic parameters are as described for Table 1.